AMERICAN UNIVERSITY OF BEIRUT

ANALYSIS OF THE HYDROGEOLOGICAL CONDITIONS AFFECTING FAULT RESPONSE TO NEARBY HYDRAULIC FRACTURING

by
DIMA JAMIL YASSINE

A thesis
submitted in partial fulfillment of the requirements
for the degree of Master of Engineering
to the Department of Mechanical Engineering
of Maroun Semaan Faculty of Engineering and Architecture
at the American University of Beirut

Beirut, Lebanon
December 2021

AMERICAN UNIVERSITY OF BEIRUT

ANALYSIS OF THE HYDROGEOLOGICAL CONDITIONS AFFECTING FAULT RESPONSE TO NEARBY HYDRAULIC FRACTURING

by

DIMA JAMIL YASSINE

Approved by:

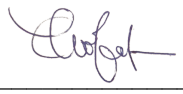

Dr. Elsa Maalouf, PhD — Advisor
Baha and Walid Bassatne Department of Chemical Engineering and Advanced Energy

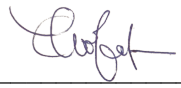

Dr. Alissar Yehya, PhD — Co-Advisor
Department of Civil and Environmental Engineering

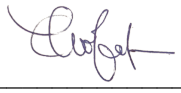

Dr. Mohamad Harb, PhD — Member of Committee
Department of Mechanical Engineering

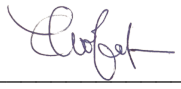

Dr. Mu'Tasem Shehadeh, PhD — Member of Committee
Department of Mechanical Engineering

Date of thesis defense: December 20, 2021

AMERICAN UNIVERSITY OF BEIRUT

THESIS RELEASE FORM

Student Name:_____Yassine_____Dima_____Jamil_____
Last First Middle

I authorize the American University of Beirut, to: (a) reproduce hard or electronic copies of my thesis; (b) include such copies in the archives and digital repositories of the University; and (c) make freely available such copies to third parties for research or educational purposes:

☐ As of the date of submission

☒ One year from the date of submission of my thesis.

☐ Two years from the date of submission of my thesis.

☐ Three years from the date of submission of my thesis.

14/1/2022

Signature Date

ACKNOWLEDGEMENTS

I would like to thank my advisor, Dr. Elsa Maalouf, for her time, efforts, and support during the past 2 years at AUB. The weekly meetings that we used to hold were of great significance in terms of guidance, input, and comments that have shaped and improved my knowledge about Geomechanics field. I appreciate Dr. Maalouf's effort in showing the path to do right research and publish articles.

I would like to express my gratitude to my co-advisor, Dr. Alissar Yehya, who invested her time, effort, and knowledge into this research. Dr. Yehya provided the initial push to accomplish this work and was always there to support, guide and help in our weekly meetings.

This work wouldn't have been completed without Dr. Maalouf's and Dr. Yehya's constant guidance, supervision, and follow-ups.

A special thanks to the committee members, Dr. Mohammad Harb and Dr. Mu'tasem Shehadeh, that provided constructive comments and highlighted some questions that helped in developing the thesis.

Finally, I would like to thank my colleague, Mahmoud Khadijeh, for his technical and moral support throughout my journey at AUB.

ABSTRACT
OF THE THESIS OF

Dima Jamil Yassine for Master of Engineering
Major: Mechanical Engineering

Title: Analysis of the Hydrogeological Conditions Affecting Fault Response to Nearby Hydraulic Fracturing

The response of critically stressed dormant faults to fluid perturbation, by oil and gas production activities, has been a major public concern because of its link to induced seismicity (IS). In this paper, we study the hydrogeological factors that affect a nearby fault response, during and after hydraulic fracturing (HF) operations, evaluated by the change in Coulomb Failure Stress (CFS) through coupling solid deformation and fluid flow. We take the Duvernay formation in Alberta, Western Canada as a base study case for our analysis. Our results show that the injection rate and the fault's distance to HF operations play an important role in increasing the CFS and hence the probability of fault reactivation. When the fault is far from the operations, its damage zones allow lateral diffusion and prevent pore pressure build up in its upper part, which stabilizes it. The lower part, however, will be under a lower normal stress and its failure may be triggered by an increase in shear stress. This is not the case of the close faults where the damage zones act as conduits for pressure diffusion and the possible triggering failure mechanism will be the increase in pore pressure. Moreover, we show that the width of the HF zone does not affect the activation mechanisms or the stability of the fault unless it is hydraulically connected to its damage zone. Therefore, serious attention should be given to the fault position, its architecture, and the volume of fluid injected to help reduce the potential for induced seismicity from HF.

TABLE OF CONTENTS

ILLUSTRATIONS

Figure

TABLES

Table

ABBREVIATIONS

CFS Coulomb Failure Stress
DZ Damaged Zone
FEM Finite Element Method
HF Hydraulic Fracturing
HFZ Hydraulically Fractured Zone
IS Induced Seismicity

CHAPTER I

INTRODUCTION

A. Introduction

With the scarcity of conventional oil and gas reserves worldwide, researchers and engineers have been trying to find economic enhancement methods that would help them extract hydrocarbons from low-permeable and tight reservoirs. Hydraulic fracturing (HF), or fracking, is a process in which a high-pressure fluid mixture is injected into a hydrocarbon bearing zone; it aims at creating new fractures and increasing the connectivity and extent of the pre-existing ones. By that, the permeability of the reservoir increases and the extraction of oil and/or gas becomes more technically feasible. Commonly, HF is done horizontally; when fracking horizontally, the surface area of contact between the well and the reservoir increases which enhances the permeability along the zone of interest. In the late 20th century, there has been a surge in combining horizontal drilling and HF especially in the US and Canada, that are known for their prominent shale reservoirs.

However, researchers have noticed that seismic events occur during and/or after certain HF operations in different regions (Bao & Eaton, 2016; Brudzinski & Kozłowska, 2019; K. Deng et al., 2016). HF can cause perturbation to the underground system and alter the pressure and stresses in the nearby pre-existing dormant faults leading to induced seismicity (IS). One of the major countries where IS by HF has been widely noticed is Canada. Canada has prominent petroleum reserves that reach up to 171 billion barrels; most of which are present in Alberta, according to the Canadian Centre for Energy Information, which have been exploited via HF. Due to the various

induced seismic events happening during and/or after HF operations in Western Canada, a Traffic Light Protocol (TLP) was implemented as a risk management measure. Operations can proceed as planned in case events under the magnitude of 2 occurred. If the magnitude of the induced events ranged between 2 and 4 within a 5 km range of the injection well, mitigation plans should be implemented while the HF operations should be ceased if the magnitude was greater than 4 (Alberta Energy Regulator, 2015).

B. Thesis Objective

Although researchers confirm that HF can induce seismic events, the mechnism(s) triggering them when fracking is still unclear. Afterall, not all HF operations lead to IS. Therefore, it is important to know the hydrogeological factors that cause the dormant faults to slip.

In this work, we aim at exploring the hydrogeological factors and perturbation mechanisms affecting faults' response during and/or after HF operations. The four factors that were studied are: the location of the faults, their orientation, the presence of a hydraulic connection between the HF zone and the faults, and the width of the damage zones. To relate the fault response to real seismic data, we consider the case study of the Duvernay formation in Alberta, Western Canada where seismic events were reported during and after operations.

C. Thesis Outline

The thesis is divided as follows. Chapter II discusses a thorough literature review about IS by HF and the possible triggering mechanisms. Chapter III describes

the methodology that is implemented that includes the case study of the Duvernay formation and the model construction. Chapters IV discusses the poroelastic theory and the governing equations. The results of the simulations are discussed and analyzed in Chapter V where different hydrogeological factors are studied to know how they affect IS by HF. Finally, the last chapter sums up and concludes on the main outcomes drawn from this work.

CHAPTER II

BACKGROUND AND LITERATURE

A. About IS

Besides natural tectonic movements, earthquakes can occur due to different anthropogenic activities. These activities that cause perturbation to the underground system can alter the pressure and stresses in the nearby dormant faults. Various case studies have attempted to understand the connection of mining (Mendecki et al., 2020) and fluid production with induced seismicity (Benson et al., 2020; Davies et al., 2013; F. Deng et al., 2020; van Thienen-Visser et al., 2018; Zbinden et al., 2017). Meanwhile, researchers have agreed on the effect of waste fluid disposal (Healy et al., 1968), geothermal systems (Bommer et al., 2006), oil and gas production (Chang & Segall, 2016; Suckale, 2009; Villa & Singh, 2020) and hydraulic fracturing (Bao & Eaton, 2016; Brudzinski & Kozłowska, 2019; K. Deng et al., 2016) on the activation of dormant faults, especially that the time of some of these operations was linked to the seismic events occurring in the respective region. Unconventional oil and gas production, including hydraulic fracturing operations, does not always induce seismic events; however, under specific geological factors, seismicity can occur even after the cessation of operations (Rashedi & Mahani, 2016). Key parameters, such as the mechanical properties of the fault and the reservoir and the in-situ conditions, can play a significant role in increasing the probability of earthquake occurrence (Van Eijs et al., 2006; Wu et al., 2017).

B. IS due to HF in Alberta, Western Canada

In low permeability formations, conventional extraction techniques cannot economically produce oil and gas from the reservoirs. Hydraulic fracturing (HF) aims at enhancing the permeability of reservoirs and, therefore, stimulating the flow of hydrocarbons into the well (Peduzzi & Harding, 2013). In shale formations, the process is done by drilling a horizontal well followed by pressurizing a limited section of the cased well by a mixture of fluids and proppants, called fracking fluid (Davis & Fisk, 2017). Seismicity can be induced during or after the high-pressure injection of fluids for formations with existing faults due to the influence of this process on the stress and strain along the fault system (Villa & Singh, 2020).

The observed surge in the rate of seismicity in North America has been mainly attributed to the massive saltwater injection into porous formation (Frohlich, 2012). Similarly, major earthquakes, whose magnitudes ranging between 2 and 6, in Alberta Canada have been linked to the hydraulic fracturing operations occurring in localized areas (Holland, 2013). Particularly, the first sequences of IS have been recorded in Fox Creek, Alberta back in 2013. According to Bao and Eaton (2016), these sequences can be connected to HF operations in the Duvernay formation since 2010. However, authors such as Atkinson et al. (2016) correlated these events spatially and temporally to the saltwater injection activities occurring in the Mississippian Debolt Formation. Bao and Eaton argued that, up to 2016, there was only one saltwater injection well in the formation where the total volume of water injected was $9.94 \times 10^4\ m^3$ (McGarr, 2014) which is a relatively small volume compared to other events induced by saltwater injection. After that, the seismicity in the Duvernay formation near Fox Creek, Alberta, CA started in 2014, during hydraulic fracturing operations, till 2015, after the cessation

of the operations (Schultz et al., 2017). The events are spatially and temporally correlated to the operations occurring in that area (Bao & Eaton, 2016).

C. Mechanisms of IS

There are two major physical mechanisms to trigger an earthquake during fluid injection. The first mechanism is the pore pressure diffusion along permeable fractures or along the damage zones of existing faults. This is mostly the case for the induced seismicity in the United States that occurred due to the injection of massive saltwater volumes into porous formations; the pore fluid pressure can diffuse for long distances until it reaches a critically stressed fault (Ellsworth, 2013; Galloway et al., 2018; Schultz et al., 2014). The second mechanism is caused by the stress changes due to the solid matrix response to injection or production (Ellsworth, 2013). Generally, there are two major factors that help nucleate an earthquake (Galloway et al., 2018): the presence of a nearly critical slip-oriented fault and a mean for stress perturbation on the fault past the critical condition. The first factor must have existed for an induced seismic event to occur (McClure & Horne, 2014). The ambiguity lies in the second factor which can be triggered by different, possibly man-induced, means. The perturbation can occur either by pore pressure diffusion that is transmitted along the damage zone (Yehya et al., 2018) or poroelastically through an impermeable rock matrix (Galloway et al., 2018) reactivating the existing faults and, therefore, releasing their stored strain energy (Walsh & Zoback, 2015). During hydraulic fracturing, the change in pore pressure alone is unlikely to induce seismic events (Bao & Eaton, 2016; K. Deng et al., 2016) because the pore pressure would require more time to diffuse along the fault and would experience changes after hours of injection, especially if the hydraulic fractures are not

directly connected to the damage zone of the fault. However, the shear and normal stresses in hydraulically fractured poroelastic medium vary instantly and significantly. Consequently, both the deformation of porous solid material and the change in pore fluid pressure (also known as poroelastic effects (Rice & Cleary, 1976)), affect the steady state of the fault (K. Deng et al., 2016). These mechanisms can trigger the earthquake at the source of the stress or pressure perturbation or deep below and away from the source. Besides, events can occur shortly after the anthropogenic activity begins or after it has been ceased. However, there exist certain hydrogeological conditions that facilitate fault reactivation (Witherspoon & Gale, 1977); these conditions need to be studied and analyzed while taking into consideration the importance of the two-way coupling between solid deformation and fluid flow.

CHAPTER III

METHODOLOGY

A. Introduction

To study the hydrogeological factors that affect IS during and after HF operations, we used the Finite Element Method (FEM) to model the case of induced seismicity in the Duvernay formation. We couple fluid flow and solid deformation to account for the poroelastic behavior and estimate the change in the Coulomb Failure Stress (CFS). We use a 2D plane strain model with a geometry inspired by the Duvernay formation case in Alberta, Canada, where induced seismicity is associated with HF. The choice of a 2D model is taken after assuming that the hydraulic fracturing operations occur around a horizontal well and affect a vertical planar region of relatively small width with respect to the domain. The main fractures propagate in this plane. Several horizontal wells are used to cover the reservoir region.

B. The Duvernay Formation

The Duvernay is an Upper Devonian mud rock containing significant quartz and carbonate which makes it an attractive Shale gas target. Lithologically, the Duvernay formation is composed of laminated bituminous shale, calcareous shale, and dense argillaceous limestone. It contains 443 trillion cubic feet of Natural Gas, 11.3 billion barrels of Natural Gas Liquids and 61.7 billion barrels of oil (Preston et al., 2016).

Irregular seismicity has been observed in the Duvernay formation in Alberta, Canada since December 2013 (Bao & Eaton, 2016). These events have been spatially and temporally correlated with the hydraulic fracturing activities occurring in the Upper Devonian Duvernay formation (Schultz et al., 2015). The link between these events and

fracking operations was controversial at that time, where some authors (Atkinson et al., 2016) correlated the events with the saltwater disposal in Mississippian Debolt formation; however, the amount of water injected was not enough to have induced the observed seismic events (McGarr, 2014).

Seismic events were observed at the end of 2014 and early January 2015 during hydraulic fracturing operations in the Duvernay formation. Even after the cessation of the operations, three sequences were also detected: S1 (January 10 till January 31), S2 (February 1 till February 18) and S3 (March 9 till March 31). The distribution of the seismic events in that cluster outlines a strike-slip system of two faults near the HF operations and with similar orientation (Bao & Eaton, 2016) as shown in **Figure 1.** The faults extend from the injection zone within the Duvernay formation into the crystalline basement. In the simulations, we will try to detect if a correlation exists between the numerically estimated positive CFS values describing the fault response and the observed seismic data.

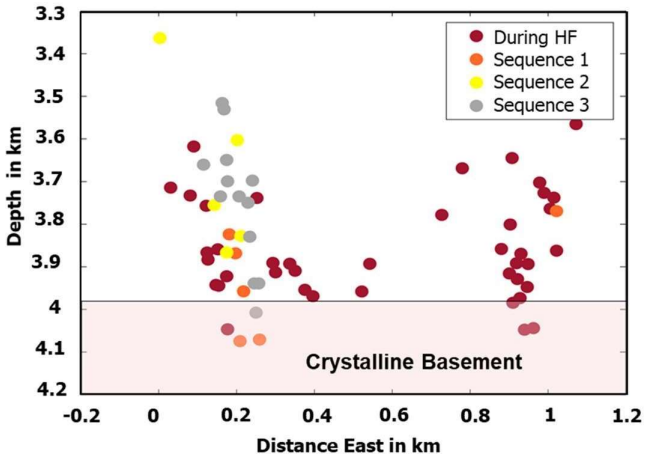

Figure 1. Cross section of a cluster showing the two strands of the fault system in the Duvernay formation (reproduced from Bao and Eaton (2016))

C. Model Construction

The entire domain is 10 km × 10 km divided into two layers inspired by the Alberta study case: The Duvernay shale (host rock) is 4 km thick, and the crystalline basement is 6 km thick as depicted in **Figure 2**. In order to simulate the stages of the fracking operations, 15 mass sources that are separated by a distance of 70 m are added at a depth of 3.4 km (Zhao, 2018) inside the hydraulic fracturing zone (**Figure 2a**). The hydraulic fracturing zone has a higher permeability than the host rock due to hydraulic fracturing and the permeability is considered to increase instantly during the operation. The fault system includes fault 1 (**Figure 2b**) that is away from the hydraulic fractures, and fault 2 (**Figure 2c**) that is directly below the hydraulic fracturing zone. Each fault has a fault core of low permeability (order of 10^{-17} m^2), and boarding damage zones of higher permeability (order of 10^{-14} m^2). The mass sources are activated one after the other by injecting 9.4 m^3/min water per mass source for 5 hours followed by 4 hours of zero-injection phase.

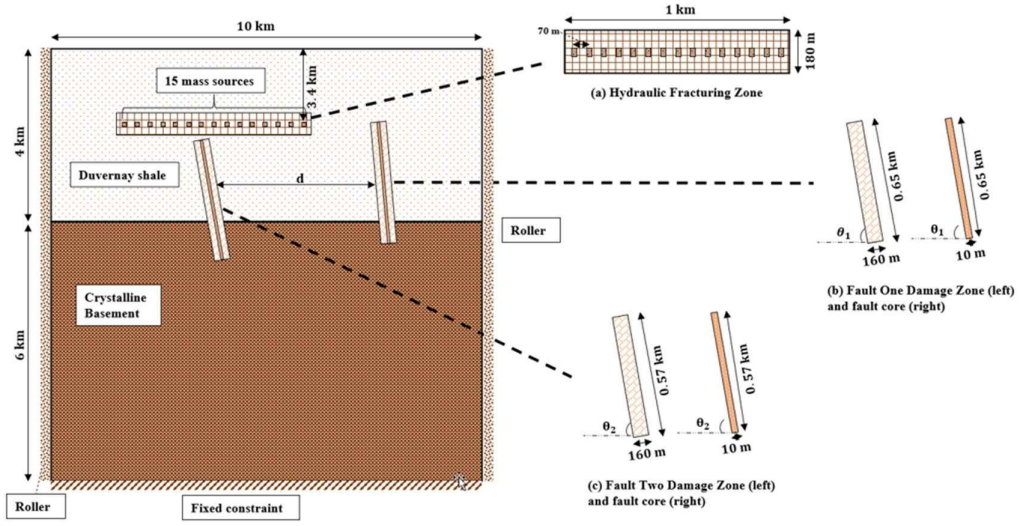

Figure 2. Model geometry with emphasis on (a) the hydraulic fracturing zone, and the geometry of (b) Fault 1 and (c) Fault 2

CHAPTER IV

THEORY AND CALCULATIONS

A. Introduction

In this section, we discuss the equations governed by the poroelastic model. This includes the coupled poroelastic model and calculations of CFS. At the end of this section, we include the initial boundary conditions that were implemented in the model.

B. Poroelastic Model and Governing Equations

1. Coulomb Stress Changes

Generally, the change in Coulomb Failure Stress (CFS) expresses the failure criterion to initiate rupture:

$$\Delta CFS = \Delta\tau + f(\Delta\sigma_n + \Delta p) \quad \ldots (1)$$

where f is coefficient of friction, taken between 0.6 and 1, $\Delta\tau$ is the change in the shear stress, $\Delta\sigma_n$ is the change applied normal stress (positive for extension) and Δp is the change in pore pressure. Any natural or anthropogenic activity that alters the shear stress, normal stress or pore pressure can bring the fault to failure and, therefore, induce an earthquake. Hence, for a critically stressed fault, as the case of most dormant faults in the subsurface, any positive change in the CFS affect the fault response to the perturbation and could lead to fault slip.

2. *Coupled Poroelastic Model*

The coupled poroelastic model states that the change in pore pressure affects the stresses and strains (fluid-to-solid coupling) and, similarly, any change in the poroelastic stresses can lead to the variation of pore pressure (solid-to-fluid) (Biot, 1941; Rice & Cleary, 1976; Wang, 2000).

The equilibrium equation, under quasi-static condition, and no additional body forces gives:

$$\nabla . \sigma = \mathbf{0} \quad \ldots (2)$$

The constitutive equation of the solid matrix when pore fluid is under pressure, with the approximation of elastic isotropy, is given by:

$$G\nabla^2 \boldsymbol{r} + \frac{G}{1-2\nu} \nabla\epsilon - \alpha\nabla p = \mathbf{0} \quad \ldots (3)$$

where $\boldsymbol{r}$ is the displacement vector, G is the shear modulus, ν is Poisson's ratio, ϵ is the volumetric strain, α is Biot-Willis coefficient and ∇p is the applied pressure gradient.

The fluid equation, derived from the conservation of mass, requires that:

$$\frac{\partial}{\partial t}(\varnothing\rho) + \nabla . (\rho \boldsymbol{u}) = Q_{\mathrm{m}} \quad \ldots (4)$$

where ρ is the density of the fluid, $\varnothing$ is the porosity of the medium, and Q_{m} is the fluid mass source.

Fluid flow in a poroelastic medium can be described by Darcy's Law where Darcy's velocity, $\boldsymbol{u}$, is expressed in terms of the permeability of the medium, κ, fluid viscosity, μ, and the difference in elevation, ∇z:

$$\boldsymbol{u} = -\frac{\kappa}{\mu}(\nabla p + \rho g \nabla z) \quad \ldots (5)$$

Furthermore, the poroelastic storage coefficient, S, is given by:

$$\frac{\partial}{\partial t}(\emptyset\rho) = \rho S \frac{\partial \rho}{\partial t} \quad \ldots (6)$$

Then, the mass conservation equation can be re-written as:

$$\rho S \frac{\partial \rho}{\partial t} + \nabla . (\rho \boldsymbol{u}) = Q_m = -\rho \alpha \frac{\partial \epsilon}{\partial t} \quad \ldots (7)$$

The negative sign in the mass source term refers to the effect of the increase of the rate of change of the volumetric strain, $\frac{\delta G}{\delta t}$. As this term increases, the fluid will sink as there is more space for the fluid to diffuse.

C. Initial Boundary Conditions

For the initial conditions, the displacement vector is null, and the pore pressure is at hydrostatic conditions. Thus, the calculated pore pressure is the excess pressure above the hydrostatic value. As for the boundary conditions for the solid matrix, we use shear-free but impenetrable boundaries for the side and bottom boundaries described as,

$$\boldsymbol{n} . \boldsymbol{u} = 0, \qquad \boldsymbol{n} \times (\boldsymbol{\sigma} . \boldsymbol{n}) = 0 \ldots (8)$$

where $\boldsymbol{u}$ is the displacement of the solid matrix, and $\boldsymbol{\sigma}$ is the stress tensor.

The top side is free to move in any direction (traction-free) (Fan et al., 2016; Segall & Lu, 2015). For the fluid flow, we assume a zero normal component of the fluid mass flux as,

$$-\boldsymbol{n} . (\rho \boldsymbol{v_f}) = 0 \ldots (9)$$

where $\boldsymbol{n}$ is the normal vector pointing outward, ρ is the fluid density, and $\boldsymbol{v_f}$ is the fluid velocity.

Table 1, **Table 2,** and **Table 3** describe the hydraulic, linear elastic and poroelastic properties of the different geological components, respectively, while **Table 4** describes the fluid properties used in the numerical models.

Table 1. Hydraulic properties of the geological components used in the numerical models

Component	**Permeability (m^2)**	**Porosity (-)**	**Reference**
Duvernay shale	1.5 E − 19	0.65	(Kleiner & Aniekwe, 2019)
Crystalline basement	10^{-21}	0.01	(Stober & Bucher, 2014)
Hydraulic fracturing zone	10^{-16}	0.1	(Rodríguez-pradilla, 2018)
Damage zones	10^{-14}	0.1	(Yehya et al., 2018)
Fault core	10^{-17}	0.015	

Table 2. Linear elastic properties of the geological components used in the numerical models

Component	**Young's Modulus (GPa)**	**Poisson's Ratio (-)**	**Density (kg/m^3)**	**Reference**
Duvernay shale	75	0.25	2700	(Zhao, 2018)
Crystalline basement	60	0.2	2750	
Damage zones	25	0.25	2700	(Gudmundsson , 2004)
Fault core	5	0.25	2700	

Table 3. Poroelastic property of the geological components used in the numerical models

Component	**Biot-Willis coefficient (-)**	**Reference**
Duvernay shale	0.79	(Fan et al., 2019)
Crystalline basement	0.44	

Table 4. Fluid properties used in the numerical models

Fluid properties	**Value**
Density (kg/m^3)	1000
Dynamic viscosity (Pa. s)	0.0004

Compressibility (1/Pa)	4 E − 10

CHAPTER V

RESULTS AND DISCUSSION

A. Introduction

In this chapter, we present the results of the poroelastic models. We mainly focus on the location of the faults, their orientation, the presence of a hydraulic connection between the HF zone and the faults, and the width of the damage zones. To assess the fault response, we estimate the change in the Coulomb Failure Stress (CFS) along two critically stressed faults, existing near the hydraulic fracturing operations using a two-dimensional finite element poroelastic model on COMSOL Multiphysics. To relate the fault response to real seismic data, we consider the case study of the Duvernay formation in Alberta, Western Canada where seismic events were reported during and after operations. The variations of the CFS along the two faults are analyzed and compared to the seismic events obtained from the observational data from December 2014 to March 2015 (Bao & Eaton, 2016). Finally, we compare the hydrogeological factors in the Duvernay formation to that of Fayetteville formation in Arkansas, US, where hydraulic fracturing operations did not induce seismic events to further link the fault response to specific favored conditions.

B. Effect of Fault Orientation

1. Vertical Faults

To accurately study the effect of fault orientation, we consider a fault system consisting of two vertical faults ($\theta_1 = \theta_2 = 0^o$) (**Figure 3**). The same model

parameters are adopted as explained in Chapter IV section C**.** The distance between Fault 1 and the hydraulic fractures is 1.01 km.

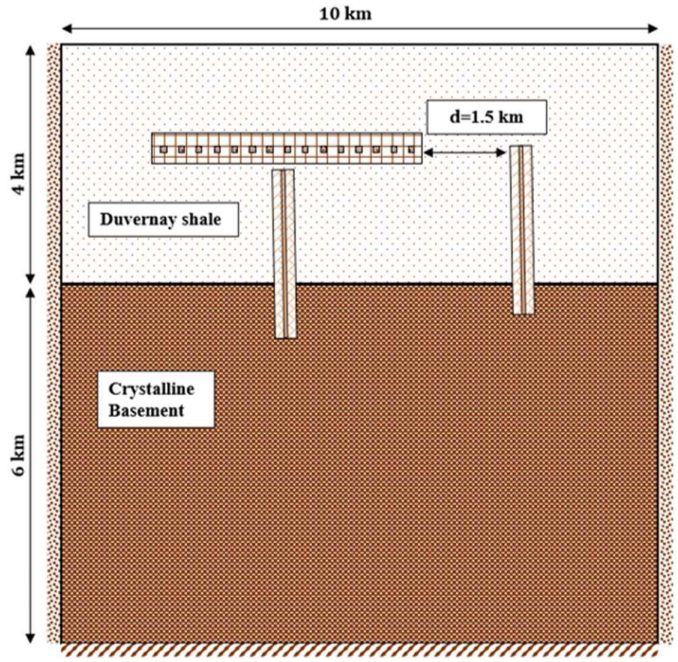

Figure 3. Model construction for vertical faults

As depicted in **Figure 4a**, Fault 1 is stabilized at the shallower parts (negative CFS) and destabilized at the deeper parts (positive CFS). The variation of the normal stress along Fault 1 in **Figure 4a** shows that the normal compressive stress at the shallower section of Fault 1 is relatively greater than that in the deeper section, leading to the state of stabilization noticed during and after HF. Additionally, the change in shear stress increases significantly with depth along Fault 1 leading to the destabilization of its deeper part. **Figure 4a** also shows the insignificant effect of pore pressure on the variation of CFS even at the later stages of the simulation. The distance between Fault 1 and the HF operations is large enough to limit a sufficient pore pressure diffusion along the fault and, hence, limit the destabilization of the fault. Therefore, the main mechanism behind the high CFS values at the deeper part of Fault 1 is the increase

in shear stress rather than pore pressure diffusion. **Figure 4b** confirms that Fault 2 shows a completely destabilizing behavior in all 4 stages. During HF, pore pressure directly diffuses along Fault 2 due to the proximity of this fault to the hydraulic fractures. However, stresses play a significant role in destabilizing Fault 2 especially at the end of HF and during S1, S2 and S3 (**Figure 4b**). Therefore, the main mechanism behind the high CFS values along Fault 1 is due to the stresses; however, both pore pressure and stresses led to the destabilization of Fault 2.

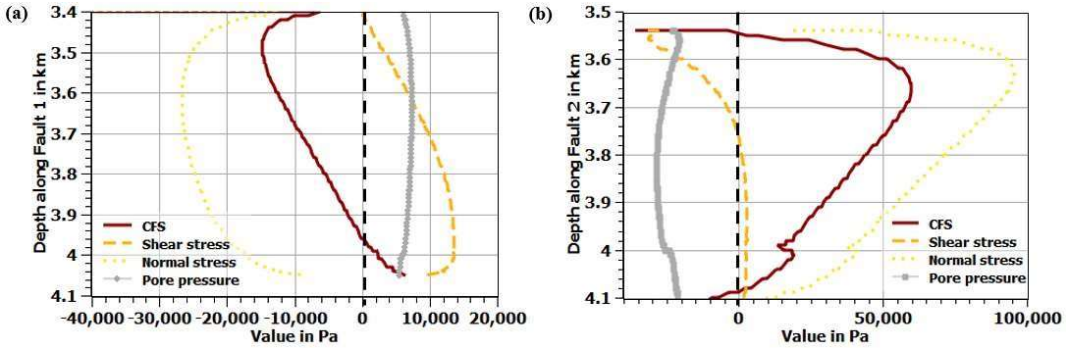

Figure 4. The variation of CFS, shear stress, normal stress, and pore pressure during HF along the vertical faults: (a) Fault 1 and (b) Fault 2

2. Oriented Faults

The orientations of the faults play a significant role in their stabilization state. To evaluate the effect of fault orientation on the change in CFS, Fault 1 and Fault 2 are oriented based on the observed seismic strands depicted in **Figure 1** where $\theta_1 = 74^0$ and $\theta_2 = 84^0$ (Bao & Eaton, 2016). The model parameters shown in **Table 1**, **Table 2** and **Table 3** are adopted and the distance between the faults is 1.5 km**.** Therefore, Fault 1 is 1.01 km away from the hydraulic fracturing operations while Fault 2 is 0.425 km below the hydraulic fractures.

Figure 5a shows the variation of the change in CFS along oriented Fault 1 during HF, S1, S2 and S3. As depicted, Fault 1 is stabilized at the shallower parts (negative CFS) and destabilized at the deeper parts (positive CFS). Error! Reference source not found.**a** shows that the shallower part of Fault 1 is subjected to a higher normal compressive stress relative to the deeper section; this leads to the destabilization of its deeper section. Error! Reference source not found.**a** shows that, even if Fault 1 was vertical, pore pressure diffusion would also be limited, and it has an insignificant effect on the variation of CFS at the later stages of the operations. The triggering failure mechanism is not altered for Fault 1 in case the orientation changed; the overall Coulomb stresses remains to be the major cause behind the destabilization of this fault. The observed seismic events (**Figure 1**) occurred solely during HF at a depth of 3.6 km, which agrees with the positive CFS values in the simulation results occurring at around a depth of 3.7 km. As for the oriented Fault 2, **Figure 5b** confirms that it is still completely destabilized during all the 4 stages. The same mechanisms attributed to the failure of the vertical Fault 2 are the same for the oriented fault (Error! Reference source not found.**b**). During HF, pore pressure directly affects the stability of Fault 2; however, by the time the operations are ceased, pore pressure has already diffused along Fault 2 and, therefore, the overall stresses are the reason behind the destabilization of the fault.

In conclusion, in case the faults were vertical, the shear stress along both faults decreases and, therefore, the faults are more stabilized in comparison to when they are oriented. In such case, Fault 1 becomes destabilized at a depth higher than 3.7 km. Similarly, Fault 2 is still completely destabilized; however, it exhibits higher values of CFS. Hence, the orientation of the faults did not affect the mechanisms of faults response but the location of the expected instability.

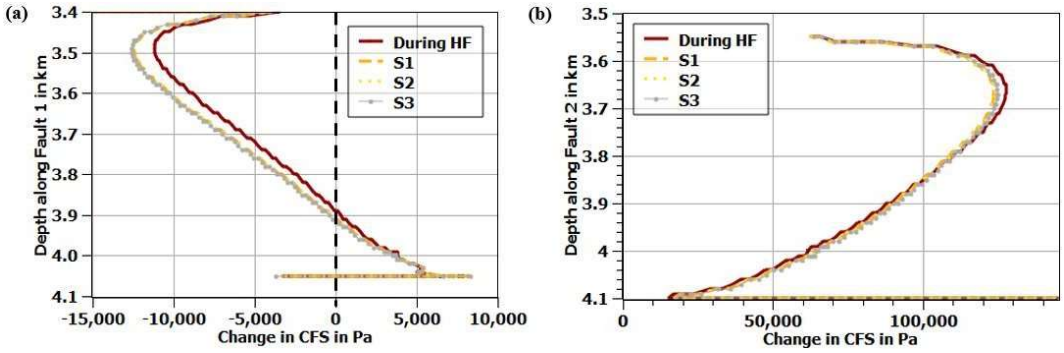

Figure 5. The variation of the CFS during the 4 stages (HF, S1, S2, S3) along the oriented faults: (a) Fault 1 and (b) Fault 2

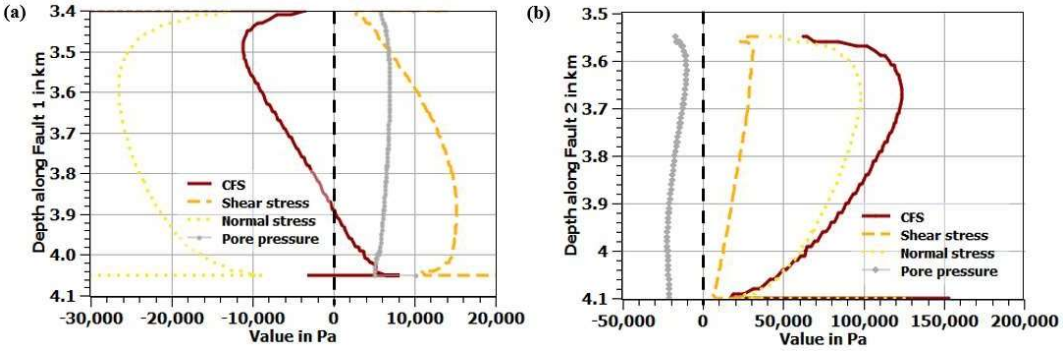

Figure 6. The variation of CFS, shear stress, normal stress, and pore pressure along (a) oriented Fault 1 during HF and (b) oriented Fault 2 during S1

C. Effect of Distance to HF Operations

We consider that the location of Fault 2 is fixed and that of Fault 1 is variable and that the distance between the last fluid mass source and Fault 1 is "d". The distance plays a significant role in destabilizing the faults as it can facilitate or delay pore pressure diffusion (Yassine et al., 2021). If Fault 1 is less than 1.01 km away from the HF operations, the fault will be affected by pore pressure diffusion caused by the

hydraulic fracturing operations. This leads to more destabilization of its shallower section. However, if Fault 1 is more than 1.01 km away from the operations, the effect of the operations will diminish. Four values for the distance between Fault 1 and the operations are adopted: $d = 0, 0.51, 1.01$ and 1.51 km. When the distance is 0 km, the fault intersects with the last hydraulic fracturing mass source (**Figure 8a**).

During the 4 stages, as Fault 1 becomes closer to the hydraulic fracturing operations, the diffusion of pore pressure is facilitated (**Figure 8**) and its CFS values become positive pointing to a destabilized response (**Figure 7a**) due to the combined effect of pore pressure and stresses. Furthermore, as this distance decreases, the normal compressive stresses at the deeper part of the fault decreases leading to its destabilizing, leaving a smaller part of the shallow section stable. This explains positive CFS values of Fault 1 presented in **Figure 7a**. When the fault intersects with the hydraulic fracturing zone, Fault 1 is completely destabilized as it is entirely under very low normal compressive stresses and relatively high pore pressure. On the contrary, if Fault 1 is 1.51 km away, most of Fault 1 is under compression and is stabilized while smaller part of its deeper section is destabilized due to a lower compressive normal stress. To observe a response that shows a stabilized upper part and destabilized lower part, which agrees with the seismic observations, the distance between Fault 1 and the operations should be around 1.01 km. As for Fault 2, the variation of CFS is barely affected by altering the distance of Fault 1 to the operations. (**Figure 7a**).

Having said that, when Fault 1 is 1.01 km away from the operations, its shallower sections are under compression and show a stabilizing behavior (i.e., negative CFS) that agrees with the lack of seismic events from observational data, and the deeper sections

of Fault 1 are under lower normal compressive stresses and show a destabilizing behavior (i.e., positive CFS), which correlates with the observed seismic events. Otherwise, the response will not correlate with the observed seismic events as Fault 1 will either be almost completely stabilized (at a distance greater than 1.51 km) or destabilized (when the fault intersects with the HF operations). Therefore, the position of the faults with respect to the location of the hydraulic fracturing operations play an important role in the mechanisms affecting the fault response leading to induced earthquakes and in their spatiotemporal distribution.

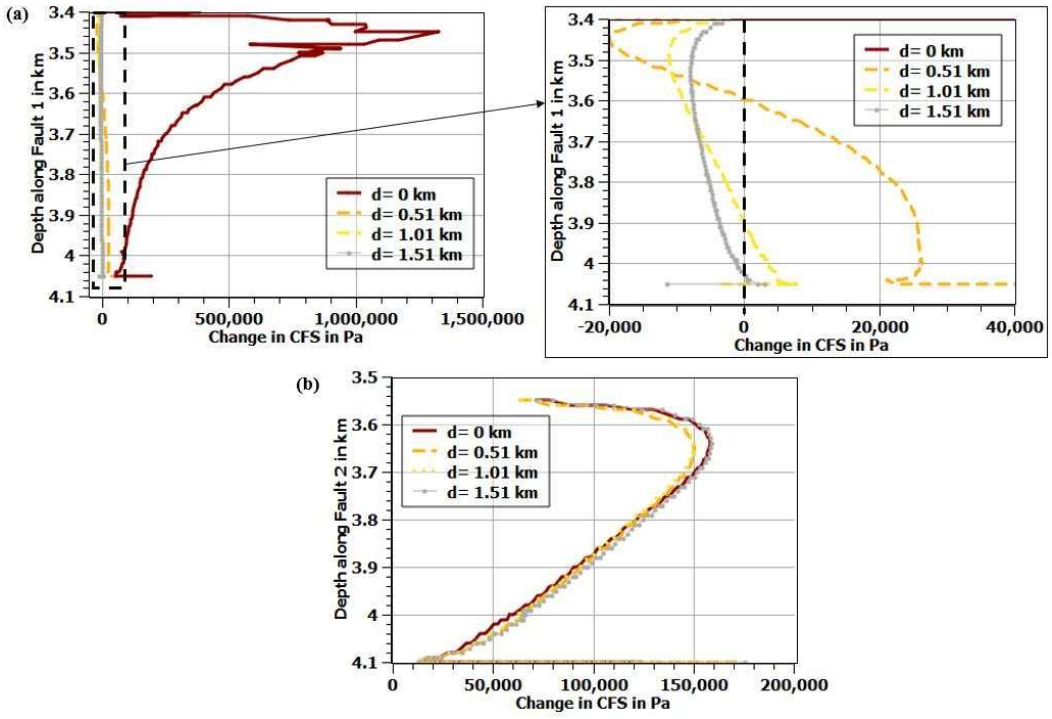

Figure 7. The variation of CFS during HF at different distances between Fault 1 and the hydraulic fractures along the oriented faults: (a) Fault 1 and (b) Fault 2

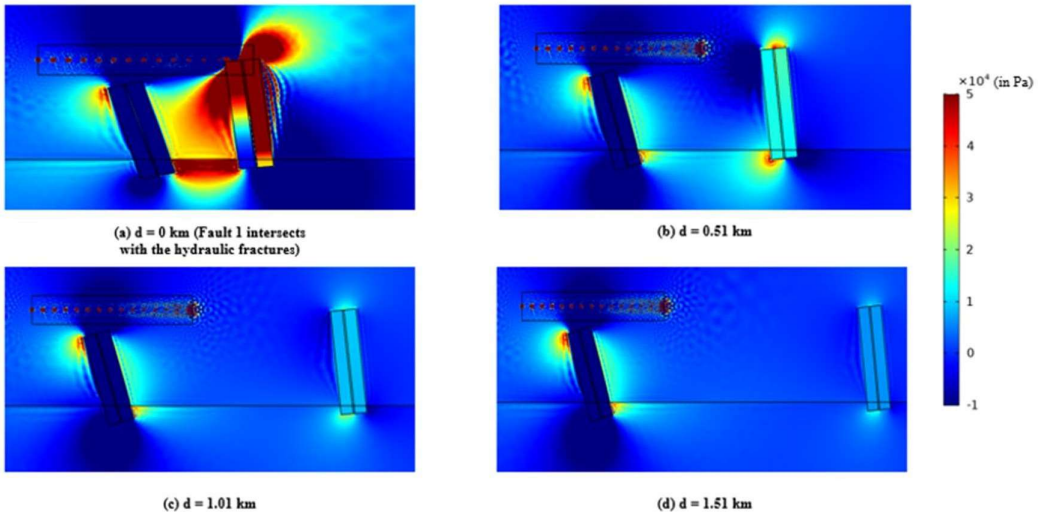

Figure 8. Colored map showing the pore pressure diffusion at the end of HF at different distances (a) d= 0 km, (b) d= 0.51 km, (c) d= 1.01 km, and (d) d= 1.51 km

D. Effect of Width Hydraulically Fractured Zone (HFZ)

To accurately simulate the effect of hydraulic fracturing operations, a zone is created around the hydraulic fractures (mass sources) which has a higher permeability and porosity than Duvernay shale. According to SM Energy company (2015), existing fractures can propagate up to 90 m because of the fluid injected at high pressures into the formation. The aim of this section is to evaluate the effect of the width of the HFZ on the variation of CFS along the critically stressed faults. We consider 3 scenarios: ignoring the permeability increase in the HF (**Figure 9a**), the HFZ, with higher permeability than the host rock, does not intersect with Fault 2 (**Figure 9b**), and the HFZ intersects with Fault 2 (**Figure 9c**). The distance between Fault 1 and the operations is considered to be 1.01 km.

Figure 10a shows the variations of CFS along Fault 2 for the 3 scenarios on the third day of HF. The highest CFS values are attained when the HFZ intersects with the damage zone of Fault 2. Since the HFZ and damage zone of Fault 2 have relatively high permeabilities (10^{-16} and $10^{-14} m^2$, respectively), the propagation of the pore pressure

is higher in comparison to when no intersection exists (**Figure 10b**). Consequently, the existence of a low permeability shale region between the hydraulically fractured zone and Fault 2 (**Figure 9a and Figure 8b**) acts as a barrier and delays the pore pressure diffusion along the fault. The slow perturbation leads to a decrease in the CFS values for cases (a) and (b) (**Figure 10a**) especially that, during HF, the main mechanism affecting the fault response of Fault 2 is the pore pressure diffusion. The presence of HFZ does not affect the CFS values of Fault 1 since Fault 1 is not destabilized during HF by a direct increase in pore pressure.

It is important to note that it is highly unlikely that there was an intersection between Fault 2 and HFZ in the real case of Duvernay formation in Alberta. According to **Figure 1**, the seismicity along Fault 2 during HF started in the deeper regions. If there was an intersection between Fault 2 and the HFZ, we expect to have seismicity start in the shallow sections.

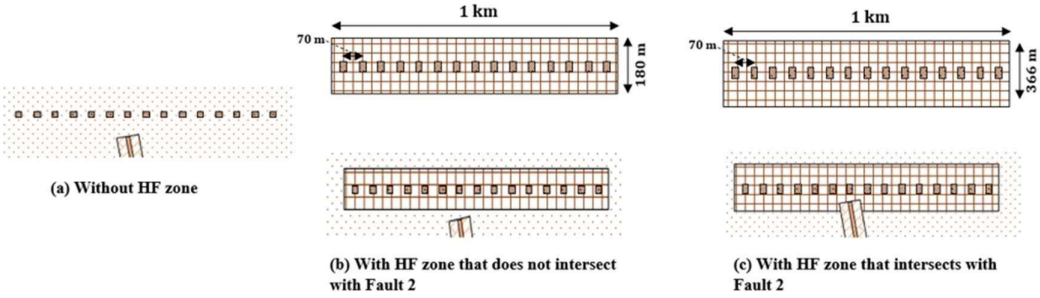

Figure 9. A close map showing the area around the hydraulic fractures and the shallow part of Fault 2 (a) without HFZ, (b) with HFZ that does not intersect with Fault 2 and (c) with HFZ that intersects with Fault 2

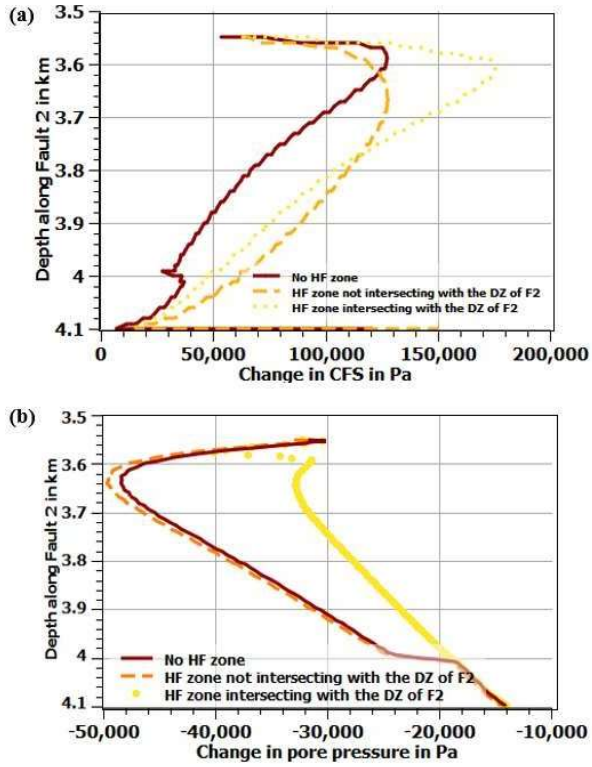

Figure 10. The variation of (a) CFS and (b) pore pressure on the third day of HF operations under different conditions: absence of HFZ (dark red), presence of HFZ that does not intersect with the damage zone (DZ) of Fault 2 (orange), and presence of HFZ that intersects with the DZ of Fault 2 (yellow)

E. Effect of Fault Architecture (width of the damage zone for Fault 1)

Depending on the location of the fluid perturbation with respect to the fault, the damage zones can play a significant role in the stabilization story. For the near fault, the damage zone plays the role of a hydraulic conduit to drive the increase in pore pressure to deeper regions of the fault. However, the width of the damage zone of the distant fault (Fault 1) might lead to decreasing the pore pressure along the fault by preventing pressure buildup and stress concentration. Therefore, four scenarios are considered where the width of the damage zone of Fault 1 (w_DZ) is varied between 0, 90, 150 and 190 m. According to **Figure 11a**, the deeper Fault 1 is more stable when the damage zone is wider. **Figure 11b** shows that the deeper section of Fault 1 is

destabilized due to high shear stress relative to the shallower section of the fault. However, as the width of the damage zone increases, the pore pressure and shear stress decrease and the deeper section of the fault becomes more stabilized. The pore pressure in Fault 1 (**Figure 11c**) is increased by the poroelastic effect and increase in the overall stresses with an indirect hydraulic connection. The more the pore fluids are trapped, the higher the pore pressure. A wider damage zone will allow a lateral diffusion resulting in the relaxation and the decrease of the pore fluid pressure around the fault. Therefore, the width of Fault 1 damage zone is expected to range between 100 and 160 m to yield a stress perturbation that is compatible with a response that correlates to the observed seismic events (stabilization during S1, S2 and S3 and destabilization of the shallow section during HF).

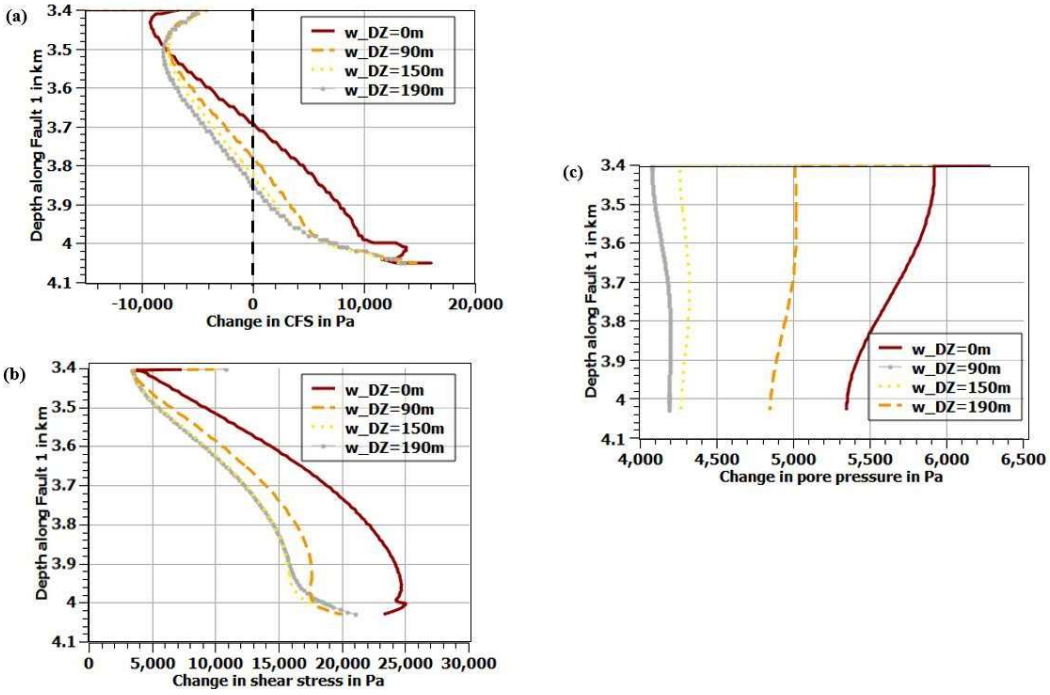

Figure 11. The variation of (a) CFS, (b) shear stress and (c) pore pressure during HF under different width of the damage zone (w_DZ) for Fault 1

F. Comparison with Fayetteville Formation

A set of geological factors could have triggered the observed seismic events in the Duvernay formation, namely the proximity to the HF operations, the fault architecture and orientation, and the injection volumes and stages. In Fayetteville formation in north-central Arkansas, U.S., no seismic events have been reported during or after the hydraulic fracturing operations. Fayetteville formation is a Mississippian black clay shale along with interbedded fine-grained limestones (McFarland, 2004). It contains around 41.6 Tcf of petroleum reserves (Arthur & Coughlin, 2008) and its age is almost equivalent to the Barnet Shale in Texas (Shelby, 2008). To compare, the total volume of fluid injected in the Fayetteville formation was around 400 m^3/cluster while it was around 2,000 m^3/cluster in the Duvernay formation. This plays a significant role in the rate and intensity of the increase in pore pressure and the stress perturbation and, therefore, the variation of CFS along the existing faults. In addition to that, the difference between the two case studies highlights the importance of the location of the existing faults relative to the hydraulic fractures. In the Fayetteville formation, two wells are operated next to a fault: one that is far (around 5 km away) and barely affects the stability of the fault and another close well whose total injected volume is very small in comparison to the Duvernay formation. Even if the hydraulic fracturing operations were close to the existing faults, the injection schedule (duration, rate, and volume of injection) plays a vital role in avoiding induced seismicity. According to Alghannam & Juanes (2020), the probability of the occurrence of seismic events increases in a shorter injection duration and a fixed injected volume as the case in the Duvernay formation.

CHAPTER VI

CONCLUSION

A. Introduction

This chapter aims at concluding with the main outcomes of this work. It focusses on the relevance of this research in the field. Finally, we suggest some future recommendations that can be implemented to better under IS due to HF.

B. Main outcomes

The rate of injection and the volume of injected fluid play a major role in induced seismicity (Alghannam & Juanes, 2020). However, for a specific injection strategy, the hydrogeological factors that have a direct effect on the pore pressure and stress perturbation along the faults are the fault orientation, distance to the operations, the width of HF zone, and the fault's architecture. These factors made the geological setting critical for induced seismicity in the Duvernay formation in Alberta. Our results show that the mechanism affecting a distant fault response, during HF, is the shear stress rather than pore pressure diffusion while both factors play a significant role in destabilizing a close Fault. When pore pressure is not the main destabilizing mechanism, the distance between the fault and the HF operations decides what part of the fault will be under a lower compressive stress and sometimes under extension, which affects its stability. Furthermore, the effect of the width of HF zone is insignificant unless it hydraulically intersects with the damage zone of a nearby fault; in that case, the pore pressure diffusion will be accelerated, and the fault will be more destabilized in the deeper section. Finally, for a distant fault i.e., where indirect fluid perturbation is happening, the width of the damage zone plays an important role in

stabilizing the fault by avoiding the pressure build up and entrapment and allowing the fluid to diffuse laterally, which leads to the decrease in shear stress and pore pressure perturbations. However, for a near fault, where direct fluid communication occurs, the damage zone plays the role of a conduit to diffuse pore pressure faster into the deeper regions of the fault.

C. Recommendation and Future Work

This work focusses on the hydrogeological factors that could trigger seismic events during and/or after HF operations. It does not properly mimic the actual HF operation and its effect on the surrounding domain. The permeability of the HFZ is assumed to be constant during the simulation time; however, this is not the real case. A better modelling to the HF operations can be adopted by increasing the permeability depending on injected fluid volume or rate. Furthermore, future work can include a model that incorporates the after-rupture effects (after the nucleation of the seismic event). In this study, over the span of 90 days, the effect of the rupture on the faults is not included which is not the case.

APPENDIX

A. Calculation of Stresses and CFS

The change in CFS is given by (Zhao and Shcherbakov, 2018),

$$\boldsymbol{CFS} = \boldsymbol{\tau} + \boldsymbol{f}(\boldsymbol{\sigma_n} + \boldsymbol{p})$$

The "Δ" is dropped in the calculation since all stresses are taken initially (at $t = 0$) to be zero.

Since the faults are assumed to be critically stressed, as the case of most faults in the subsurface, any positive change in CFS, is likely to induce a seismic event.

The normal stress, σ_n, and shear stress, τ, are expressed as

$$\boldsymbol{\sigma_n} = \boldsymbol{\sigma_{ij} n_i n_j} \ldots (10)$$

$$\boldsymbol{\sigma_n} = \boldsymbol{\sigma_{11} n_1 n_1} + \boldsymbol{\sigma_{22} n_2 n_2} + \boldsymbol{\sigma_{33} n_3 n_3} + \boldsymbol{2\sigma_{12} n_1 n_2} + \boldsymbol{2\sigma_{23} n_2 n_3} + \boldsymbol{2\sigma_{13} n_1 n_3} \ldots (11)$$

$$\boldsymbol{\tau} = ((\boldsymbol{T_i^n})^2 + (\boldsymbol{T_i^n})^2 + (\boldsymbol{T_i^n})^2 - \boldsymbol{\sigma_n^2})^{\frac{1}{2}} \ldots (12)$$

$$\boldsymbol{T_i^n} = \boldsymbol{\sigma_{ij} n_j} \ldots (13)$$

$$\boldsymbol{\tau} = \{[\boldsymbol{\sigma_{11} n_1} + \boldsymbol{\sigma_{12} n_2} + \boldsymbol{\sigma_{13} n_3}]^2 + [\boldsymbol{\sigma_{12} n_1} + \boldsymbol{\sigma_{22} n_2} + \boldsymbol{\sigma_{23} n_3}]^2 + [\boldsymbol{\sigma_{13} n_1} + \boldsymbol{\sigma_{23} n_2} + \boldsymbol{\sigma_{33} n_3}]^2 - \boldsymbol{\sigma_n^2}\}^{\frac{1}{2}} \ldots (14)$$

where n_i is the normal vector to the fault plane

$$\boldsymbol{n_1} = -\boldsymbol{sin\theta\ sin\gamma} \ldots (15)$$

$$\boldsymbol{n_2} = -\boldsymbol{sin\theta\ cos\gamma} \ldots (16)$$

$$\boldsymbol{n_3} = \boldsymbol{cos\gamma} \ldots (17)$$

where θ is the fault dip and γ is the fault strike

Table 5 shows the detailed calculations of the stresses and CFS in a 2D model.

Table 5. Summary of equations used in 2D

	Vertical Faults	**Faults with orientation**
n_1	$\mathbf{1}$	$\boldsymbol{sin\theta}$
n_2	$\mathbf{0}$	$\mathbf{0}$
n_3	$\mathbf{0}$	$\mathbf{0}$
σ_n	$\boldsymbol{\sigma_n = \sigma_{11}}$	$\boldsymbol{\sigma_n = \sigma_{11} n_1^2}$
τ	$\boldsymbol{\tau = \sigma_{12}}$	$\boldsymbol{\tau = [\sigma_{11}^2 n_1^2 + \sigma_{12}^2 n_1^2 - \sigma_{11}^2 n_1^4]^{\frac{1}{2}}}$
CFS	$\boldsymbol{\sigma_{12} + f\,\sigma_{11} + f\,p}$	$\boldsymbol{[\sigma_{11}^2 n_1^2 + \sigma_{12}^2 n_1^2 - \sigma_{11}^2 n_1^4]^{\frac{1}{2}} + f\,\sigma_{11} n_1^2 + f\,p}$

REFERENCES

Alghannam, M., & Juanes, R. (2020). Understanding rate effects in injection-induced earthquakes. *Nature Communications*, *11*(1), 1–6. https://doi.org/10.1038/s41467-020-16860-y

Arthur, D. J., & Coughlin, B. J. (2008). *Hydraulic Fracturing Considerations for Natural Gas Wells of the Fayetteville Shale*. 1–19. internal-pdf://arthur_fayetteville-0032732421/Arthur_Fayetteville.pdf

Atkinson, G. M., Eaton, D. W., Ghofrani, H., Walker, D., Cheadle, B., Schultz, R., Shcherbakov, R., Tiampo, K., Gu, J., Harrington, R. M., Liu, Y., Van Der Baan, M., & Kao, H. (2016). Hydraulic fracturing and seismicity in the western Canada sedimentary basin. *Seismological Research Letters*, *87*(3), 631–647. https://doi.org/10.1785/0220150263

Bao, X., & Eaton, D. W. (2016). Fault activation by hydraulic fracturing in western Canada. *Science*, *354*(6318), 1406–1409. https://doi.org/10.1126/science.aag2583

Benson, P. M., Austria, D. C., Gehne, S., Butcher, E., Harnett, C. E., Fazio, M., Rowley, P., & Tomas, R. (2020). Laboratory simulations of fluid-induced seismicity, hydraulic fracture, and fluid flow. *Geomechanics for Energy and the Environment*, *24*, 100169. https://doi.org/10.1016/j.gete.2019.100169

Biot, M. A. (1941). General theory of three-dimensional consolidation. *Journal of Applied Physics*, *12*(2), 155–164. https://doi.org/10.1063/1.1712886

Bommer, J. J., Oates, S., Cepeda, J. M., Lindholm, C., Bird, J., Torres, R., Marroquín, G., & Rivas, J. (2006). Control of hazard due to seismicity induced by a hot fractured rock geothermal project. *Engineering Geology*, *83*(4), 287–306. https://doi.org/10.1016/j.enggeo.2005.11.002

Brudzinski, M. R., & Kozłowska, M. (2019). Seismicity induced by hydraulic fracturing and wastewater disposal in the Appalachian Basin, USA: a review. *Acta Geophysica*, *67*(1), 351–364. https://doi.org/10.1007/s11600-019-00249-7

Chang, K. W., & Segall, P. (2016). Injection-induced seismicity on basement faults including poroelastic stressing. *Journal of Geophysical Research: Solid Earth*, *121*(4), 2708–2726. https://doi.org/10.1002/2015JB012561

Davies, R., Foulger, G., Bindley, A., & Styles, P. (2013). Induced seismicity and hydraulic fracturing for the recovery of hydrocarbons. *Marine and Petroleum Geology*, *45*, 171–185. https://doi.org/10.1016/j.marpetgeo.2013.03.016

Davis, C., & Fisk, J. M. (2017). Mitigating Risks From Fracking-Related Earthquakes: Assessing State Regulatory Decisions. *Society and Natural Resources*, *30*(8), 1009–1025. https://doi.org/10.1080/08941920.2016.1273415

Deng, F., Dixon, T. H., & Xie, S. (2020). Surface Deformation and Induced Seismicity Due to Fluid Injection and Oil and Gas Extraction in Western Texas. *Journal of Geophysical Research: Solid Earth*, *125*(5), 1–22. https://doi.org/10.1029/2019JB018962

Deng, K., Liu, Y., & Harrington, R. M. (2016). Poroelastic stress triggering of the December 2013 Crooked Lake, Alberta, induced seismicity sequence. *Geophysical Research Letters*, *43*(16), 8482–8491. https://doi.org/10.1002/2016GL070421

Ellsworth, W. L. (2013). *Injection-Induced Earthquakes*. *341*(July), 1–8.

Fan, Z., Eichhubl, P., & Gale, J. F. W. (2016). Geomechanical analysis of fluid injection and seismic fault slip for the Mw4.8 Timpson, Texas, earthquake sequence. *Journal of Geophysical Research: Solid Earth*, *April 2008*, 3782–3803. https://doi.org/10.1002/2015JB012608.Received

Fan, Z., Eichhubl, P., & Newell, P. (2019). Basement Fault Reactivation by Fluid Injection Into Sedimentary Reservoirs: Poroelastic Effects. *Journal of Geophysical Research: Solid Earth*, *124*(7), 7354–7369. https://doi.org/10.1029/2018JB017062

Frohlich, C. (2012). Two-year survey comparing earthquake activity and injection-well locations in the Barnett Shale, Texas. *Proceedings of the National Academy of Sciences of the United States of America*, *109*(35), 13934–13938. https://doi.org/10.1073/pnas.1207728109

Galloway, E., Hauck, T., Corlett, H., Pană, D., & Schultz, R. (2018). Faults and associated karst collapse suggest conduits for fluid flow that influence hydraulic fracturinginduced seismicity. *Proceedings of the National Academy of Sciences of the United States of America*, *115*(43), E10003–E10012. https://doi.org/10.1073/pnas.1807549115

Gudmundsson, A. (2004). Effects of Young's modulus on fault displacement. *Comptes Rendus - Geoscience*, *336*(1), 85–92. https://doi.org/10.1016/j.crte.2003.09.018

Healy, J. H., Rubey, W. W., Griggs, D. T., & Raleigh, C. B. (1968). The Denver Earthquakes. Disposal of waste fluids by injection into a deep well has riggered earthquakes near Denver, Colorado. In *Science* (Vol. 161, Issue 3848, pp. 1301–1310).

Holland, A. A. (2013). Earthquakes triggered by hydraulic fracturing in south-central Oklahoma. *Bulletin of the Seismological Society of America*, *103*(3), 1784–1792. https://doi.org/10.1785/0120120109

Kleiner, S., & Aniekwe, O. (2019). The Duvernay Shale completion journey. *Society of Petroleum Engineers - SPE Kuwait Oil and Gas Show and Conference 2019, KOGS 2019*, 1–7. https://doi.org/10.2118/198070-ms

McClure, M. W., & Horne, R. N. (2014). Correlations between formation properties and induced seismicity during high pressure injection into granitic rock. *Engineering Geology*, *175*, 74–80. https://doi.org/10.1016/j.enggeo.2014.03.015

McFarland, J. D. (2004). Stratigraphic Summary of Arkansas. In *Arkansas Geological Survey Information Circular* (Vol. 36, p. 44). http://www.geology.ar.gov/info_circulars/ic36.htm

McGarr, A. (2014). Journal of Geophysical Research : Solid Earth. *AGU: Journal of Geophysical Research, Solid Earth*, *119*, 3678–3699. https://doi.org/10.1002/2013JB010597.Received

Mendecki, M. J., Szczygieł, J., Lizurek, G., & Teper, L. (2020). Mining-triggered seismicity governed by a fold hinge zone: The Upper Silesian Coal Basin, Poland. *Engineering Geology*, *274*(June). https://doi.org/10.1016/j.enggeo.2020.105728

Peduzzi, P., & Harding, R. (2013). Gas fracking: can we safely squeeze the rocks? *Environmental Development*, *6*(November), 86–99. https://doi.org/10.1016/j.envdev.2012.12.001

Preston, A., Garner, G., & Beavis, K. (2016). *Duvernay Reserves and Resources Report*. *December*.

Rashedi, H., & Mahani, A. (2016). *Data Analysis of Induced Seismicity in Western Canada*. *2*, 26–28.

Rice, J. R., & Cleary, M. P. (1976). Some basic stress diffusion solutions for fluid-saturated elastic porous media with compressible constituents. *Reviews of Geophysics*, *14*(2), 227–241. https://doi.org/10.1029/RG014i002p00227

Rodríguez-pradilla, G. (2018). Reservoir Characterization of a Duvernay-Fox Creek Shale Reservoir using Seismic , Microseismic , and Well Log Data. *CSEG*

Recorder, *June*, 30–34.

Schultz, R., Stern, V., & Gu, Y. J. (2014). An investigation of seismicity clustered near the Cordel Field, west central Alberta, and its relation to a nearby disposal well. *Journal of Geophysical Research: Solid Earth*, *119*(4), 3410–3423. https://doi.org/10.1002/2013JB010836

Schultz, R., Stern, V., Novakovic, M., Atkinson, G., & Gu, Y. J. (2015). Hydraulic Fracturing and the Crooked Lake Sequences: Insights Gleaned From Regional Seismic Networks. *Geophysical Research Letters*, 261–308. https://doi.org/10.1007/978-3-319-21314-9_8

Schultz, R., Wang, R., Gu, Y. J., Haug, K., & Atkinson, G. (2017). A seismological overview of the induced earthquakes in the Duvernay play near Fox Creek, Alberta. *Journal of Geophysical Research: Solid Earth*, *122*(1), 492–505. https://doi.org/10.1002/2016JB013570

Segall, P., & Lu, S. (2015). Injection-induced seismicity: Poroelastic and earthquake nucleation effects. *Journal of Geophysical Research: Solid Earth*, *120*(7), 5082–5103. https://doi.org/10.1002/2015JB012060

Shelby, P. (2008). *The Fayetteville Shale Play of North-Central Arkansas – A Project Update*. http://www.geology.ar.gov/info_circulars/ic36.htm

Stober, I., & Bucher, K. (2014). *Hydraulic conductivity of fractured upper crust: insights from hydraulic tests in boreholes and ?uid-rock interaction in crystalline basement rocks*. 2019–2021. https://doi.org/https://doi.orh.10.1111/gfl.12104

Suckale, J. (2009). Induced Seismicity in Hydrocarbon Fields. *Advances in Geophysics*, *51*(C), 55–106. https://doi.org/10.1016/S0065-2687(09)05107-3

Van Eijs, R. M. H. E., Mulders, F. M. M., Nepveu, M., Kenter, C. J., & Scheffers, B. C.

(2006). Correlation between hydrocarbon reservoir properties and induced seismicity in the Netherlands. *Engineering Geology*, *84*(3–4), 99–111. https://doi.org/10.1016/j.enggeo.2006.01.002

van Thienen-Visser, K., Roholl, J. A., van Kempen, B. M. M., & Muntendam-Bos, A. G. (2018). Categorizing seismic risk for the onshore gas fields in the Netherlands. *Engineering Geology*, *237*(March 2017), 198–207. https://doi.org/10.1016/j.enggeo.2018.02.004

Villa, V., & Singh, R. P. (2020). Hydraulic fracturing operation for oil and gas production and associated earthquake activities across the USA. *Environmental Earth Sciences*, *79*(11), 1–11. https://doi.org/10.1007/s12665-020-09008-0

Walsh, F. R., & Zoback, M. D. (2015). Oklahoma's recent earthquakes and saltwater disposal. *Science Advances*, *1*(5). https://doi.org/10.1126/sciadv.1500195

Wang, H. F. (2000). Theory of linear poroelasticity with applications to geomechanics and hydrogeology. *Princeton University Press*.

Witherspoon, P. A., & Gale, J. E. (1977). Mechanical and hydraulic properties of rocks related to induced seismicity. *Engineering Geology*, *11*(1), 23–55. https://doi.org/10.1016/0013-7952(77)90018-7

Wu, J. H., Liao, C. J., Lin, H. M., & Fang, T. T. (2017). An experimental study to characterize the initiation of the seismic-induced Tsaoling rock avalanche. *Engineering Geology*, *217*, 110–121. https://doi.org/10.1016/j.enggeo.2016.12.015

Yassine, D., Yehya, A., & Maalouf, E. (2021). Numerical Analysis of the Induced Seismicity Triggered by Hydraulic Fracturing in the Duvernay Formation in Alberta, CA. *EGU General Assembly 2021.* https://doi.org/10.5194/egusphere-egu21-4740, 2021

Yehya, A., Yang, Z., & Rice, J. R. (2018). Effect of Fault Architecture and Permeability Evolution on Response to Fluid Injection. *Journal of Geophysical Research: Solid Earth*, *123*(11), 9982–9997. https://doi.org/10.1029/2018JB016550

Zbinden, D., Rinaldi, A. P., Urpi, L., & Wiemer, S. (2017). On the physics-based processes behind production-induced seismicity in natural gas fields. *Journal of Geophysical Research: Solid Earth*, *122*(5), 3792–3812. https://doi.org/10.1002/2017JB014003

Zhao, B. (2018). Geomechanical Modelling of Induced Seismicity. *Thesis*, *August*.